Materials Science and Engineering C 64 (2016) 243–248

Contents lists available at ScienceDirect

Materials Science and Engineering C

journal homepage: www.elsevier.com/locate/msec

A novel biosensor based on the direct electrochemistry of horseradish peroxidase immobilized in the three-dimensional flower-like Bi_2WO_6 microspheres

Hui Liu *, Kai Guo [1], Congyue Duan [1], Xianjin Chen, Zhenfeng Zhu

School of Materials Science and Engineering, Shaanxi University of Science and Technology, Xi'an 710021. PR China

ARTICLE INFO

Article history:
Received 26 January 2016
Received in revised form 18 March 2016
Accepted 22 March 2016
Available online 24 March 2016

Keywords:
Biosensor
Enzyme immobilization
Bi_2WO_6
Three-dimensional flower-like microspheres
Hydrogen peroxide

ABSTRACT

Three-dimensional flower-like Bi_2WO_6 microspheres (3D-Bi_2WO_6 MSs) have been synthesized through a simple hydrothermal method. The morphology and structure of 3D-Bi_2WO_6 MSs were characterized by scanning electron microscopy (SEM) and X-ray diffraction (XRD). The 3D-Bi_2WO_6 MSs subsequently were used to immobilize horseradish peroxidase (HRP) and fabricate a mediator-free biosensor for the detection of H_2O_2. Spectroscopic and electrochemical results reveal that 3D-Bi_2WO_6 MSs constitute an excellent immobilization matrix with biocompatibility for enzymes. Meanwhile, due to unique morphology of the flower-like microspheres, the direct electron transfer of HRP is facilitated and the prepared biosensors display good performances for the detection of H_2O_2 with a wide linear range, including two linear sections: 0.5–100 μM ($R^2 = 0.9983$) and 100–250 μM ($R^2 = 0.9981$), as well as an extremely low method detection limit of 0.18 μM.

1. Introduction

Recent researches show that nanomaterials modified electrode has special effect on electrocatalysis and electrochemical determination [1–4]. Especially in system contained many kinds of similar substrate, some electrodes have selective detection or simultaneously detection [5–8]. Meanwhile, nanomaterial can play an important and unique role in direct electrochemical biosensor [9–14]. The researches of direct electron transfer (DET) of enzymes or redox proteins can not only help to understand the intrinsic kinetic and thermodynamic properties of proteins but also establish a foundation for fabricating mediator-free biosensors [15,16]. However, it is difficult for proteins to realize the DET process on the bare electrode, due to the deep burying of electroactive center in the protein structure and the denaturation of proteins on the bare electrode surface [17,18]. Recent studies show that a series of nanomaterials with good biocompatibility and special surface effect can be used to immobilize enzymes and fabricate mediator-free biosensors [18,19]. Among them, three-dimensional (3D) structured nanomaterials, such as 3D nanostructured NiO [19], ZnO [20], TiO_2 [21], MnO_2 [17] microspheres and $Co(OH)_2$ macroporous film [22], have received increasing attention for their unique structure and morphology. It has been shown that the structure and morphology of nanomaterials have a significant effect on the property of the immobilized enzyme, which determines their efficacy in biosensors [23]. So finding new nanomaterials with special morphology and structure possessing high biosensor performance is still a challenge.

To the best of our knowledge, 3D structured Bi_2WO_6 nanomaterial as a support for constructing mediator-free biosensor has rarely been reported. Here, three-dimensional flower-like Bi_2WO_6 microspheres (3D-Bi_2WO_6 MSs) were synthesized by a simple hydrothermal method. This kind of 3D-Bi_2WO_6 MSs possess many advantages as a support for immobilization of enzyme. As shown in Scheme 1, numerous nanosheets, all pointing toward the center of the sphere, constitute the 3D-Bi_2WO_6 MSs which own a large surface area available for enzyme entrapment. And the trumpet-shaped pores among the nanosheets can become tunnels to the interior of the microsphere for enzymes. Furthermore, the nanosheets are formed from numerous smaller nanosheets (<100 nm in length) which can greatly enhance the active surface area for adsorbing enzymes (Fig. S1). Meanwhile, the substrate has easy access to the enzymes immobilized in the microspheres through the trumpet-shaped pores. Concentration of substrate and enzyme in this confined region will increase the chance of effective collisions between them [24]. Hence, such kind of 3D-Bi_2WO_6 MSs are able to become a promising support for enzyme immobilization and have potential applications in biosensors.

In this study, horseradish peroxidase (HRP) is selected as a model redox protein for construction of the biosensor. Meanwhile, to highlight the advantages of the 3D-Bi_2WO_6 MSs, Bi2WO6 nanoparticles (Bi_2WO_6 NPs) are also used as a support to immobilize HRP.

* Corresponding author.
E-mail address: liuhui@sust.edu.cn (H. Liu).
[1] These authors contributed equally to this work.

http://dx.doi.org/10.1016/j.msec.2016.03.079
0928-4931/

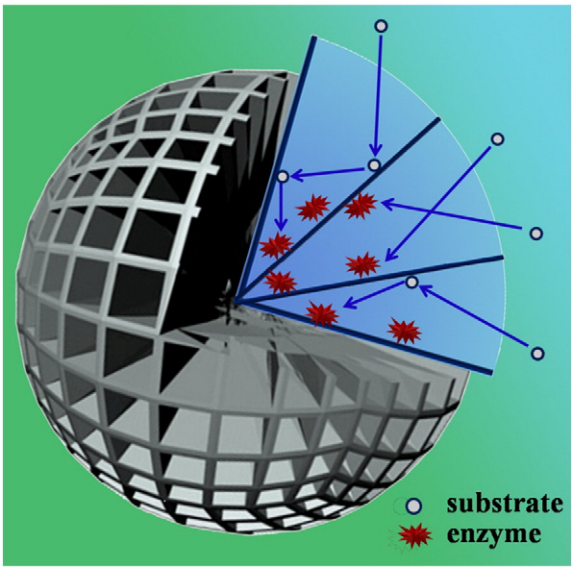

Scheme 1. Schematic illustration of the 3D-Bi_2WO_6 MSs immobilizing HRP.

2. Experimental

2.1. Materials and apparatus

HRP and Nafion were purchased from Sigma (St. Loius, MO, USA). Other chemical reagents were purchased from Sinopharm Chemical Reagent Co., Ltd., China. All reagents are analytical grade. In all experiments, deionized water was used.

Field-emission scanning electron microscopy (FE-SEM) was performed using a Hitachi S-4800 & Hiroba energy dispersive X-ray electron microscope (Hitachi, Japan). X-ray diffraction (XRD) patterns were recorded on a Rigaku D/max 2200pc diffractometer (Rigaku, Japan) using Cu Kα radiation of wavelength $\lambda = 0.15418$ nm at 40 kV and 40 mA. UV–vis spectra were recorded using a PerkinElmer Lambda-950 spectrophotometer (PerkinElmer, America). FT-IR spectra were obtained on a Bruker TENSOR27 instrument (Bruker, Germany). Zeta potential was performed by a Malvern Nano-Z system (Malvern, England). All electrochemical experiments were performed with a CHI 660E electrochemical workstation (CH Instruments, China). A conventional three-electrode system, which consisted of a platinum wire as the counter electrode, an Ag/AgCl/3M KCl as the reference electrode and a 3-mm diameter modified glassy carbon electrode (GCE) as the working electrode, was used in all electrochemical experiments. Unless otherwise noted, 0.1 M phosphate buffered saline (PBS; pH 7.0) was used as the supporting electrolyte in all experiments. The buffer was purged with highly purified nitrogen for at least 30 min and a nitrogen atmosphere environment was kept in electrochemical measurements.

2.2. Synthesis of 3D-Bi_2WO_6 microspheres

The 3D-Bi_2WO_6 microspheres were synthesized by a facile hydrothermal reaction. In a typical synthesis, the starting materials of $Na_2WO_4 \cdot 2H_2O$ and $Bi(NO_3)_3 \cdot 5H_2O$ with the stoichiometric ratio were added into 30 mL deionized water with stirring for 10 min, respectively. Then the $Na_2WO_4 \cdot 2H_2O$ solution was added with drop by drop to the $Bi(NO_3)_3 \cdot 5H_2O$ suspension. After stirring for 30 min, the obtained white suspension was loaded into a 100 mL Teflon-liner autoclave and then treated for 12 h at 180 °C. The products were washed with deionized water and absolute ethanol to remove any ionic residue then dried at 60 °C.

2.3. Preparation of enzyme electrode

Prior to use, a glassy carbon electrode (GCE) was polished with 0.3 and 0.05 μm alumina slurry and sonicated in ethanol and water successively. The cleaned GCE was dried using a purified nitrogen stream. The enzyme electrode was prepared by a simple casting method. Firstly, 1 mL of 2 mg mL^{-1} 3D-Bi_2WO_6 suspension and 0.5 mL of 10 mg mL^{-1}HRP PBS were mixed and stirred for 20 min. Secondly, 0.5 mL of Nafion (5%) was added to the mixture and then stirred for 10 min. Finally, 4 μL of the mixture was applied to the surface of a freshly polished GCE to prepare the Nafion/HRP/3D-Bi_2WO_6/GCE and then stored in refrigerator prior to use. To compare, Bi_2WO_6 nanoparticles (Bi_2WO_6 NPs) were used for the fabrication of Nafion/HRP/Bi_2WO_6 NPs/GCE with similar procedures as described above. In the control experiment, Nafion/HRP/GCE and Nafion/3D-Bi_2WO_6/GCE were also prepared. Before electrochemical measurements, all the as-prepared film electrodes were immersed in pH 7.0 PBS for 30 min to remove residual components.

3. Results and discussions

3.1. Characterization of 3D-Bi_2WO_6 MSs

X-ray diffraction (XRD) is firstly used to determine the structure and crystallinity of the as-prepared products. Fig. 1 shows the XRD pattern of the products. The peaks in this diffraction pattern correspond to the orthorhombic Bi_2WO_6 crystal phase (JCPDS No. 73–2020). The XRD pattern also indicates that the prepared Bi_2WO_6 sample has a high crystallinity.

As shown in Fig. 2A and B, the 3D-Bi_2WO_6 MSs with the diameter of about 4 μm are composed of numerous nanosheets pointing toward the center of the sphere. The trumpet-shaped pores among the nanosheets can become tunnels to the interior of the microsphere for enzymes. Furthermore, from the higher-magnification SEM image (the inset of Fig. 2B), the nanosheets are formed from numerous smaller nanosheets (<100 nm in length). This special structure can greatly enhance the active surface area for enzymes adsorption.

Fig. 2C depicts the microstructure image of Nafion/HRP/3D-Bi_2WO_6 composite film. It is noted that 3D-Bi_2WO_6 MSs is discernible on the surface of modified electrode. The 3D-Bi_2WO_6 MSs is embedded in the Nafion to form a stable composite film which is essential for the stability of the prepared enzyme electrode. Moreover, because of the high surface area of 3D-Bi_2WO_6 MSs, the effective surface area of the modified electrode improves greatly (Fig. 2D).

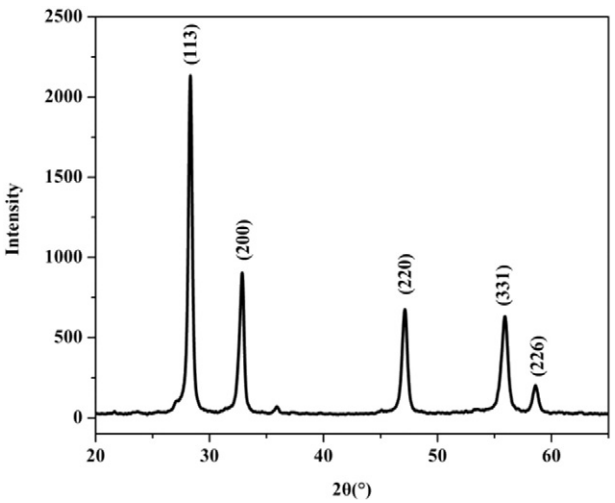

Fig. 1. XRD pattern of the 3D-Bi_2WO_6 MSs.

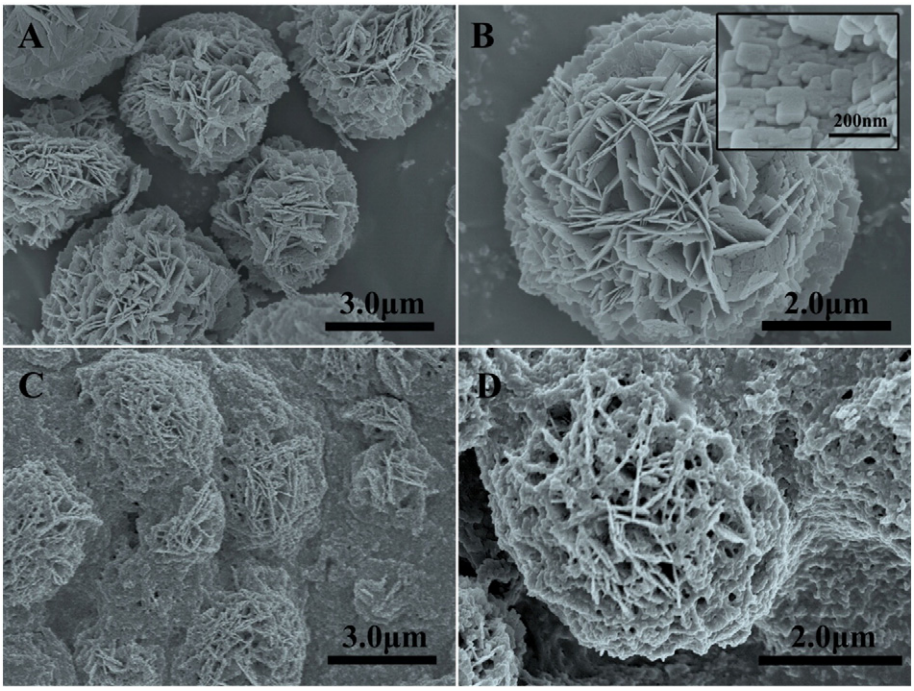

Fig 2. SEM images of typical as-synthesized 3D-Bi_2WO_6 MSs (A and B) and Nafion/HRP/3D-Bi_2WO_6 composite film (C and D).

Fig. S1 gives the typical SEM images of 3D-Bi_2WO_6 MSs (A) and HRP/3D-Bi_2WO_6 MSs (3D-Bi_2WO_6 MSs immobilizing HRP) (B). It can be clearly seen from the comparison that the special three-dimensional flower-like structure and the rough surfaces of Bi_2WO_6 microspheres can greatly enhance the active surface area for enzymes adsorption.

3.2. Encapsulation of HRP in the of Nafion/3D-Bi_2WO_6 composite film

Zeta potential measurement shows that the prepared 3D-Bi_2WO_6 MSs carry negative charges with a zeta potential of −15.3 mV. The isoelectric point (pI) of enzymes decides the surface electrical property of enzymes in solution. As we known, the pI of HRP (pI = 8.9 [25]) is larger than pH 7.0. Hence, when pH (solution)≤7.0, the surface of HRP carries positive charge. Thus, positively charged HRP molecules in pH 7.0 PBS can be attached onto the3D-Bi_2WO_6 MSs surface by the electrostatic interaction.

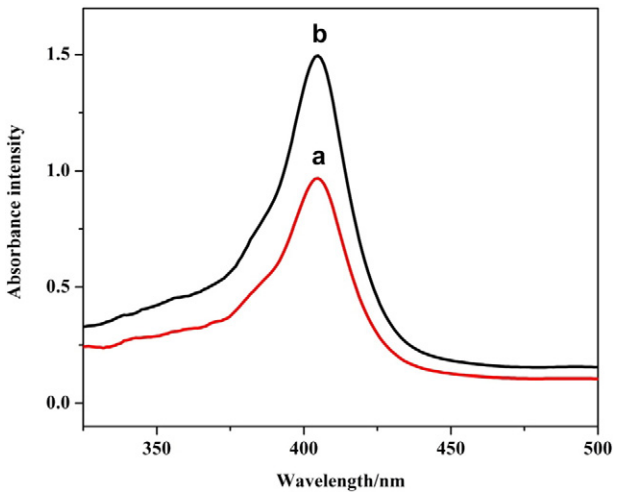

Fig. 3. UV–vis spectra of Nafion/HRP/3D-Bi_2WO_6 composite film (a) and HRP (b).

UV–vis spectroscopy is an effective method to monitor the structure change of heme proteins. The Soret absorption bands of heme proteins provide information about the conformational integrity of the enzymes [26,27]. As shown in Fig. 3, the Soret absorption band of HRP immobilized on Nafion/HRP/3D-Bi_2WO_6 (storage at 4 °C for four weeks) is located at 407 nm (curve a), which is close to that of native HRP at 409 nm (curve b), indicating that HRP retained the essential features of its conformational integrity. This reveals that Nafion/3D-Bi_2WO_6 composite film has biocompatibility and do not suffer significant enzymes denaturation.

3.3. Direct electrochemistry behavior of Nafion/HRP/3D-Bi_2WO_6/GCE

Fig. 4 depicts the typical cyclic voltammograms (CVs) of different modified electrodes in 0.1 M PBS (pH 7.0) at a scan rate of 0.1 V s^{-1}.

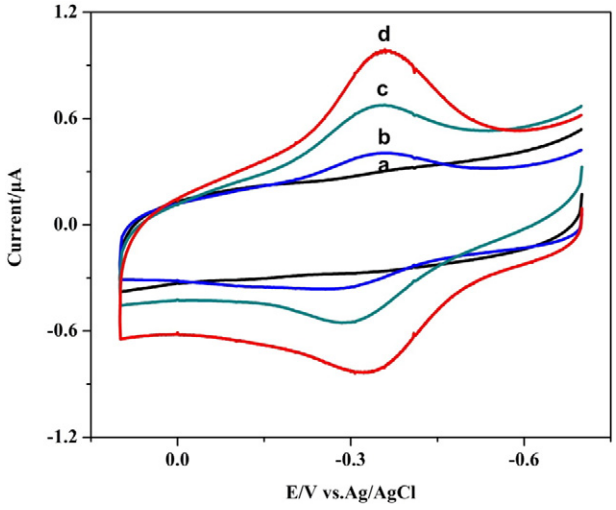

Fig. 4. Cyclic voltammograms of Nafion/3D-Bi_2WO_6/GCE (a), Nafion/HRP/GCE (b), Nafion/HRP/Bi_2WO_6NPs/GCE (c), Nafion/HRP/3D-Bi_2WO_6/GCE (d), in 0.1 M pH 7.0 PBS with a scan rate of 0.1 V s^{-1}.

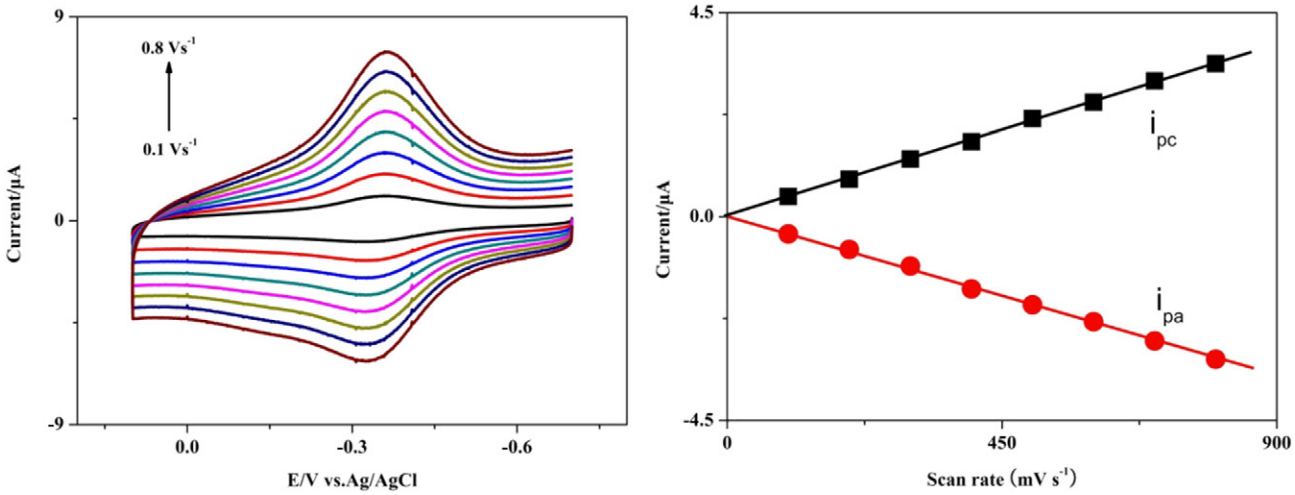

Fig. 5. Cyclic voltammograms of Nafion/HRP/3D-Bi_2WO_6/GCE in 0.1 M pH 7.0 PBS with increasing scan rates from 0.1 to 0.8 Vs^{-1} (A), plot of cathodic and anodic peak current vs. scan rate (B).

No redox peak is observed at Nafion/3D-Bi_2WO_6/GCE (curve a), which indicates that Nafion/3D-Bi_2WO_6/GCE is electroinactive in the potential window. The Nafion/HRP/3D-Bi_2WO_6/GCE (curve d) exhibits a couple of stable and well-defined redox peaks at −0.367 V and −0.323 V vs. Ag/AgCl, which could be ascribed to direct electron transfer between HRP and the underlying electrode. According to Li et al. [28], the electron transfer of HRP occurs between the Fe^{III} and Fe^{II} site within HRP. The formal potential ($E^{0'} = (E_{p,a} + E_{p,c}) / 2$) of HRP is −0.345 V vs. Ag/AgCl is in agreement with −0.335 V, −0.362 V and −0.369 V vs. Ag/AgCl reported for the HRP($Fe^{III/II}$) redox couple in HRP-ZrP, HRP-graphene-Nafion and HRP-GO-Nafion films [28–30]. The potential difference (ΔE_p) between the anodic and cathodic peak potential is about 44 mV. Such a small ΔE_p value reveals a fast and quasi-reversible electron-transfer process, and then indicates that the 3D-Bi_2WO_6 MSs can provide a favorable microenvironment for HRP to undergo a facile electron-transfer reaction. Compared with that of the Nafion/HRP/3D-Bi_2WO_6/GCE, almost no redox peaks are observed at the Nafion/HRP/GCE (curve b, in Fig. 4), suggesting an enhanced electron transfer between HRP molecules and the surface of the Nafion/HRP/3D-Bi_2WO_6/GCE. Meanwhile, due to the deep burying of electroactive center in the protein structure and the denaturation of proteins on the bare electrode surface, it is difficult for proteins to realize the DET process on the bare electrode [31]. It can be clearly seen from the comparison that direct electron transfer between HRP molecules and GCE is greatly enhanced at the Nafion/HRP/3D-Bi_2WO_6/GCE. For comparison, Nafion/HRP/Bi_2WO_6NPs/GCE has also been carried out (curve c, in Fig. 4). The reduction peak of the electrode is 45.8% smaller than that of Nafion/HRP/3D-Bi_2WO_6/GCE. The ΔE_p is 68 mV, which is larger than that of Nafion/HRP/3D-Bi_2WO_6/GCE (44 mV), indicating faster electron transfer rate of HRP on the electrode than on Nafion/HRP/Bi_2WO_6NPs/GCE. It can be concluded that 3D-Bi_2WO_6 MSs have better effect on the facilitation of electron transfer, which may result from unique morphology and property of the 3D-Bi_2WO_6 MSs.

Fig. 5A shows the cyclic voltammograms of Nafion/HRP/3D-Bi_2WO_6/GCE at 0.1 M PBS (pH 7.0) with the scan rate increasing from 0.1 to 0.8 V s^{-1}. With the increasing of the scan rate, the cathodic and anodic peak currents of HRP increase simultaneously. Meanwhile, the cathodic and anodic peak potentials show a slight shift respectively lead to the peak to peak separation slightly enlarged. Fig. 5B shows that the cathodic (i_{pc}) and anodic (i_{pa}) peak currents increase linearly with scan rates from 0.1 to 0.8 V s^{-1}. This reveals that the electrode reaction corresponds to a surface-controlled quasi-reversible process. By using the Laviron method for a surface-controlled electrochemical system [29], the apparent heterogeneous electron transfer rate constant (k_s) of HRP immobilized on Nafion/HRP/3D-Bi_2WO_6/GCE is estimated to be about 3.4 s^{-1}, which is higher than the value reported for HRP immobilized β-cyclodextrin hybrid film (2.87 s^{-1}) [32], flowerlike ZnO-gold nanoparticle-Nafion nanocomposite (1.94 s^{-1}) [33], suggesting a faster electron-transfer process. This means that the 3D-Bi_2WO_6 MSs facilitate the direct electron transfer of HRP. The average surface concentration of electroactive HRP (Γ^*, mol cm^{-2}) can be estimated from the charge integration of the reduction peak of the CV using the formula:

$$Q = nFA\Gamma* \quad (1)$$

where F is Faraday constant, Q is the charge (C) and can be obtained by integrating the reduction peak of HRP, n and A stand for the number of electron transferred and the geometrical surface area of the electrode, respectively. According to this method, the surface concentration of electroactive HRP (Γ^*) at Nafion/HRP/3D-Bi_2WO_6/GCE is calculated as 1.13×10^{-10} mol cm^{-2}, which is much greater than the theoretical value for monolayer coverage (1.89×10^{-11} mol cm^{-2}) [34]. This means that multilayers of HRP entrapped in the Nafion/HRP/3D-Bi_2WO_6/GCE participates in the electron-transfer process.

Fig. 6 shows the cyclic voltammograms of 0.1 M PBS of different pH at a Nafion/HRP/3D-Bi_2WO_6/GCE. Stable and well-defined CVs are observed in the pH range 6.0–8.0. With the increasing of pH value, both the cathodic and anodic peaks shift to the negative (Fig. 6). This can

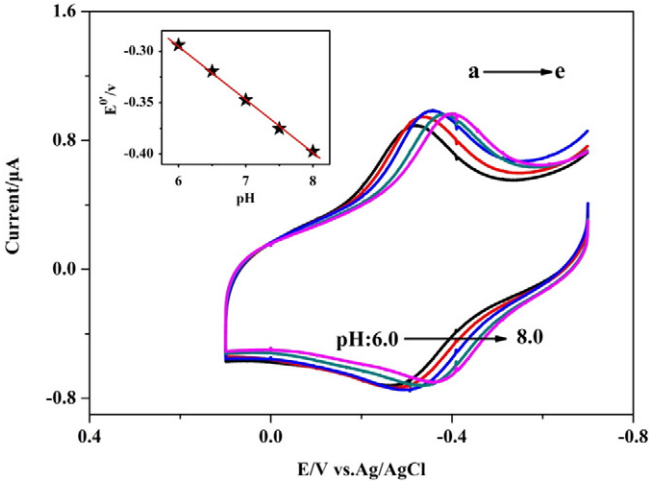

Fig. 6. Cyclic voltammograms of Nafion/HRP/3D-Bi_2WO_6/GCE in 0.1 M PBS with different pH values from 6 to 8. Inset: plot of cathodic and anodic peak current vs. pH values.

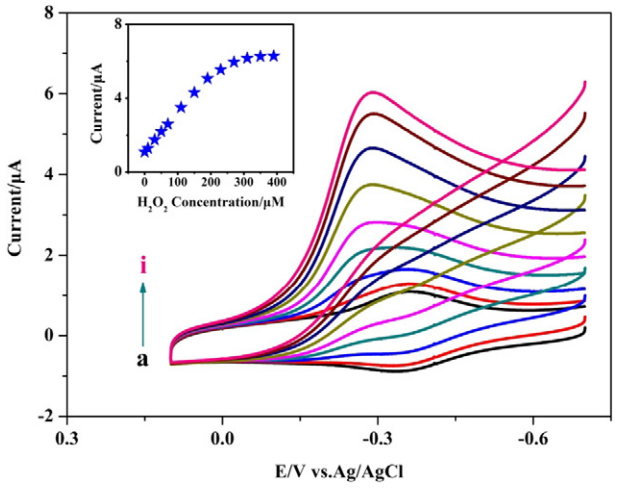

Fig. 7. Cyclic voltammograms of the Nafion/HRP/3D-Bi_2WO_6/GCE in 0.1 M pH 7.0 PBS containing 0 (a), 10 (b), 30 (c), 50 (d), 70 (e), 110 (f), 150 (g), 190 (h), 230 (i) μM H_2O_2 at a scan rate of v = 0.1 V s^{-1}. Inset: plot of the relationship between catalytic reduction current and the concentration of H_2O_2.

be contributed to the involvement of proton transfer in the HRP(Fe^{III})/HRP(Fe^{II}) redox couple [35]. The $E^{0'}$ value of HRP varies linearly in the range of pH 6.0–8.0, with a slop of −52.5 mV pH^{-1} (the inset of Fig. 6). This value is very close to the theoretical value of the transfer of one proton and electron in a reversible reduction (−58 mV pH^{-1} at 25 °C) [36].

3.4. Electrocatalytic properties of the Nafion/HRP/3D-Bi_2WO_6/GCE

By using H_2O_2 as a probe, the electrocatalytic properties of the Nafion/HRP/3D-Bi_2WO_6/GCE were investigated. As shown in Fig. 7, the reduction peak increases dramatically with the addition of H_2O_2, accompanied by a decrease and disappearance of the oxidation peak, displaying the obvious electrocatalytic behavior of HRP for the reduction of H_2O_2 [27]. A possible reaction mechanism of H_2O_2 catalyzed by the HRP-based electrode is postulated as follows [28]:

$$HRP\left(Fe^{III}\right) + e^{-} \rightleftharpoons HRP\left(Fe^{II}\right) \quad (2)$$

Table 1
Determination results of H_2O_2 in real samples.

Samples	$KMnO_4$ titration (mM)	This work (mM)	Added (mM)[a]	Found (mM)[b]	Recovery (%)
1	0.17	0.17	0.10	0.26	96.3
2	0.13	0.14	0.10	0.25	104.1
3	0.14	0.15	0.10	0.24	96.0

[a] Standard H_2O_2 solution added to the samples.
[b] The total concentrations of H_2O_2 after addition of standard H_2O_2 solution to the samples.

$$HRP\left(Fe^{II}\right) + H_2O_2 + 2H^{+} \rightarrow HRP\left(Fe^{III}\right) + 2H_2O. \quad (3)$$

With the H_2O_2 concentration increasing, the current value reaches a saturation limit (the inset of Fig. 7) and saturation behavior is characteristic of enzyme-based catalysis. The apparent Michaelis-Menten constant (K_M^{app}) can be obtained by the electrochemical-version of Lineweaver-Burk equation [37]

$$\frac{1}{I_{ss}} = \frac{K_M^{app}}{I_{max}C} + \frac{1}{I_{max}} \quad (4)$$

where I_{ss} is the steady-state current after the addition of substrate, C is the bulk concentration of the substrate, and I_{max} is the maximum current measured under saturated substrate conditions. The K_M^{app} value for Nafion/HRP/3D-Bi_2WO_6/GCE is estimated to be 153 μM. This value is smaller than those ever reported values of 262 μM [26] and 684 μM [30], indicating that HRP immobilized on Nafion/HRP/3D-Bi_2WO_6/GCE retains higher bioactivity.

3.5. Biosensor performance of the Nafion/HRP/3D-Bi_2WO_6/GCE

The biosensor performance for the detection of H_2O_2 of the Nafion/HRP/3D-Bi_2WO_6/GCE was also investigated by amperometry. Fig. 8 gives the amperometric responses of the modified glassy carbon electrodes at −0.35 V after adding H_2O_2 in stirred PBS (pH 7.0). Fig. 8A demonstrates that, on Nafion/HRP/3D-Bi_2WO_6/GCE, the response time (achieving 95% of the steady-state current) is <3 s. Fig. 8B shows two linear sections in the calibration plots. The first section is from 0.5 to 100 μM with a correlation coefficient of 0.9983 (N = 14), and the other is from 100 to 250 μM with a correlation coefficient of 0.9987 (N = 16). The method detection limit is estimated

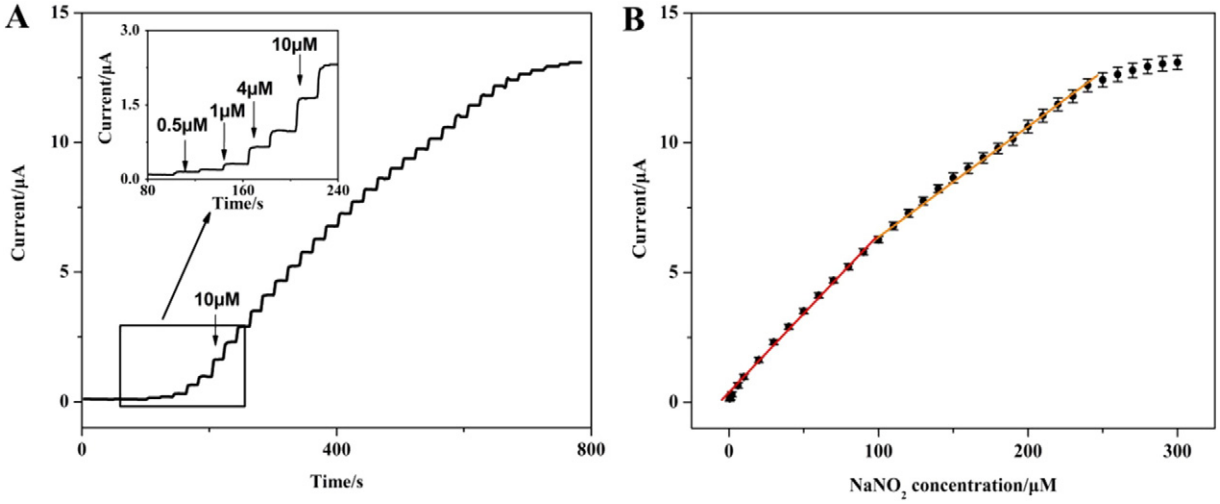

Fig. 8. Amperometric response curves of the Nafion/HRP/3D-Bi_2WO_6/GCE to H_2O_2. Applied potential: −0.35 V (A). Plot of steady-state response currents against concentrations of H_2O_2 (B).

to be 0.18 μM (the signal to noise ratio is 3). Performances of various H_2O_2 biosensors are listed in Table S1. It is clear that the performance of Nafion/HRP/3D-Bi_2WO_6/GCE is significantly improved. Furthermore, compared with Nafion/HRP/Bi_2WO_6NPs/GCE, the 3D-Bi_2WO_6 based biosensor has better performance (Fig. S2). There are some reasons why the Nafion/HRP/3D-Bi_2WO_6/GCE displays both a lower method detection limit and a wider linear range. Firstly, this kind of three-dimensional flower-like Bi_2WO_6 microspheres can greatly enhance the active surface area for enzymes' adsorption. More importantly, the substrate can simply be entrapped by 3D-Bi_2WO_6 MSs with larger specific surface area and the special flower-like structure, and have easy access to the enzymes immobilized on the surface of 3D-Bi_2WO_6 MSs. There is an increased chance of effective collisions between substrate and redox protein leading to improved performance of this sensor [24].

3.6. Stability and reproducibility of the biosensor

The long-term stability of the fabricated biosensors was studied by examining its current response after storage at 4 °C. The biosensors can retain 93.1% of the initial response to H_2O_2 after 30-day storage, demonstrating good long-term stability (Fig. S3). The good long-term stability can be contributed to the good biocompatibility of 3D-Bi_2WO_6 MSs which can provide a favorable microenvironment for HRP to retain its bioactivity.

The reproducibility of the biosensor was investigated by determining 5 μM H_2O_2 in PBS (pH 7.0). The relative standard deviation (R.S.D) is 3.2% for 5 successive measurements. Five biosensors prepared under the same conditions independently give a R.S.D. of 3.8% for the determination of 5 μM H_2O_2 in PBS (0.1 M, pH 7.0), indicating an acceptable electrode-to-electrode reproducibility.

3.7. Analysis of real samples

In order to evaluate the analytical utility of the electrode in practice, the Nafion/HRP/3D-Bi_2WO_6/GCE is applied for determination of real contact lens care solution. Before experiments, the real samples are diluted 5000 times with doubly distilled water and without any other pretreatments. Recovery tests and $KMnO_4$ titration method were used to examine the reliability and accuracy of this method. The H_2O_2 content of different samples and recoveries of added analyte are evaluated, and the results confirm that determining the H_2O_2 concentration in real samples by using the proposed method is reliable (Table 1)."

4. Conclusion

In summary, three-dimensional flower-like Bi_2WO_6 microspheres have been synthesized through a simple hydrothermal method and subsequently are used to fabricate a mediator-free biosensor for the detection of H_2O_2. Due to unique morphology of the flower-like microspheres, the Nafion/HRP/3D-Bi_2WO_6/GCE biosensor displays a low method detection limit of 0.18 μM and a wide linear range from 0.5 to 250 μM for H_2O_2.

Acknowledgments

This work was financially supported by the National Science Foundation of China (51272147), the Natural Science Foundation of Shaanxi Province (2015JM5208) and the Graduate Innovation Fund of Shaanxi University of Science and Technology.

Appendix A. Supplementary data

Supplementary data to this article can be found online at http://dx.doi.org/10.1016/j.msec.2016.03.079.

References

[1] H. Beitollahi, M.M. Ardakani, B. Ganjipour, H. Naeimi, Biosens. Bioelectron. 24 (2008) 362–368.
[2] H. Hosseini, M. Behbahani, M. Mahyari, H. Kazerooni, A. Bagheri, A. Shaabani, Biosens. Bioelectron. 59 (2014) 412–417.
[3] M.K. Bojdi, M.H. Mashhadizadeh, M. Behbahani, A. Farahani, S.S.H. Davarani, A. Bagheri, Electrochim. Acta 136 (2014) 59–65.
[4] M.K. Bojdi, M. Behbahani, M.H. Mashhadizadeh, A. Bagheri, S.S.H. Davarani, A. Farahani, Materials Science and Engineering: C 48 (2015) 213–219.
[5] E. Molaakbari, A. Mostafavi, H. Beitollahi, R. Alizadeh, Analyst 139 (2014) 4356–4364.
[6] H. Beitollahi, H. Karimi-Maleh, H. Khabazzadeh, Anal. Chem. 80 (2008) 9848–9851.
[7] H. Beitollahi, I. Sheikhshoaie, Electrochim. Acta 56 (2011) 10259–10263.
[8] H. Beitollahi, I. Sheikhshoaie, J. Electroanal. Chem. 661 (2011) 336–342.
[9] M. Baghayeri, H. Veisi, Biosens. Bioelectron. 74 (2015) 190–198.
[10] M. Baghayeri, E.N. Zare, M.M. Lakouraj, Biosens. Bioelectron. 55 (2014) 259–265.
[11] M. Baghayeri, E.N. Zare, R. Hasanzadeh, Mater. Sci. Eng. C 39 (2014) 213–220.
[12] M. Baghayeri, RSC Adv. 5 (2015) 18267–18274.
[13] M. Baghayeri, H. Veisi, H. Veisi, B. Maleki, H. Karimi-Maleh, H. Beitollahi, RSC Adv. 4 (2014) 49595–49604.
[14] M. Baghayeri, E.N. Zare, M.M. Lakouraj, Sensors Actuators B Chem. 202 (2014) 1200–1208.
[15] C. Léger, S.J. Elliott, K.R. Hoke, L.J. Jeuken, A.K. Jones, F.A. Armstrong, Biochemistry 42 (2003) 8653–8662.
[16] I. Hamachi, A. Fujita, T. Kunitake, J. Am. Chem. Soc. 119 (1997) 9096–9102.
[17] Z. Zhu, L. Qu, Q. Niu, Y. Zeng, W. Sun, X. Huang, Biosens. Bioelectron. 26 (2011) 2119–2124.
[18] Q.-L. Sheng, J.-B. Zheng, X.-D. Shang-Guan, W.-H. Lin, Y.-Y. Li, R.-X. Liu, Electrochim. Acta 55 (2010) 3185–3191.
[19] S. Dong, P. Zhang, H. Liu, N. Li, T. Huang, Biosens. Bioelectron. 26 (2011) 4082–4087.
[20] X. Lu, H. Zhang, Y. Ni, Q. Zhang, J. Chen, Biosens. Bioelectron. 24 (2008) 93–98.
[21] H. Tao, J. Wang, Y. Ou, W. Zhu, H. Ling, W. Fang, D. Tu, Nanosci. Nanotechnol. Lett. 6 (2014) 99–105.
[22] Q. Xie, X. Chen, H. Liu, W. Yang, Sensors Actuators B Chem. 168 (2012) 277–282.
[23] J. Kim, J.W. Grate, P. Wang, Chem. Eng. Sci. 61 (2006) 1017–1026.
[24] Q. Xie, Y. Zhao, X. Chen, H. Liu, D.G. Evans, W. Yang, Biomaterials 32 (2011) 6588–6594.
[25] G.-X. Wang, W.-J. Bao, J. Wang, Q.-Q. Lu, X.-H. Xia, Electrochem. Commun. 35 (2013) 146–148.
[26] X. Chen, C. Fu, Y. Wang, W. Yang, D.G. Evans, Biosens. Bioelectron. 24 (2008) 356–361.
[27] S. Mao, Y. Long, W. Li, Y. Tu, A. Deng, Biosens. Bioelectron. 48 (2013) 258–262.
[28] M. Li, S. Xu, M. Tang, L. Liu, F. Gao, Y. Wang, Electrochim. Acta 56 (2011) 1144–1149.
[29] X. Yang, X. Chen, L. Yang, W. Yang, Bioelectrochemistry 74 (2008) 90–95.
[30] L. Zhang, H. Cheng, H.-m. Zhang, L. Qu, Electrochim. Acta 65 (2012) 122–126.
[31] H. Liu, C. Duan, C. Yang, X. Chen, W. Shen, Z. Zhu, Mater. Sci. Eng. C 53 (2015) 43–49.
[32] A. Cao, H. Ai, Y. Ding, C. Dai, J. Fei, Sensors Actuators B Chem. 155 (2011) 632–638.
[33] C. Xiang, Y. Zou, L.-X. Sun, F. Xu, Sensors Actuators B Chem. 136 (2009) 158–162.
[34] S.-F. Wang, T. Chen, Z.-L. Zhang, X.-C. Shen, Z.-X. Lu, D.-W. Pang, K.-Y. Wong, Langmuir 21 (2005) 9260–9266.
[35] X. Chen, Q. Wang, L. Wang, F. Gao, W. Wang, Z. Hu, Biosens. Bioelectron. 66 (2015) 216–223.
[36] F. Wu, J. Xu, Y. Tian, Z. Hu, L. Wang, Y. Xian, L. Jin, Biosens. Bioelectron. 24 (2008) 198–203.
[37] R.A. Kamin, G.S. Wilson, Anal. Chem. 52 (1980) 1198–1205.